Facile synthesis and complete characterization of $Zn_{1-x}Sr_xAl_2O_4$ ($0 \leq x \leq 0.5$) spinel nanoparticles using combustion technique

R. Jothiramalingam[a*], K. Mathankumar[b], M. Sundararajan[c], M. Sukumar[d], J. A. Dhanraj[e], R. Divya[f], H. A. Al-Lohedan[a], M. Chandrasekaran[g], D. M. Al-Dhayan[a]

[a]*Chemistry Department, College of Science, King Saud University, P.O. Box 2455, Riyadh 11451, Saudi Arabia.*

[b]*Department of Science and Humanities, St. Michael College of Engineering and Technology, Kalaiyarkoil 630551, Tamilnadu, India*

[c]*PG & Research Department of Physics, Paavendhar College of Arts & Science, M.V. South, Attur, Salem 636 121,Tamilnadu, India*

[d]*Department of Physics, Anand Institute of Higher Technology, Kazhipattur, Chennai, 603103, India*

[e]*Department of Mechanical Engineering, Hindustan University, Rajiv Gandhi Salai (OMR), Padur, Kelambakam, Chennai, Tamil Nadu 603103, India*

[f]*Department of Physics, Science and Humanities. SMK Forma Institute of Technology, Kelambakkam 603 103, India*

[g]*Department of Food Science and Biotechnology, Sejong University, Gwangjin-gu, Seoul -05006, South Korea*

$Zn_{1-x}Sr_xAl_2O_4$ ($0 \leq x \leq 0.5$) nanoparticles are successfully produced by combustion method. Powder XRD studies confirms the substitution of Sr^{2+} in $ZnAl_2O_4$ spinel nanostructure and average crystallite size lies between 32 to 39 nm. FTIR spectra revealed bands at 710 and 563 cm^{-1} corresponds to the intrinsic stretching vibrations of M_{tetra}–O atom which takes place at tetrahedral lattice sites and octahedral metal stretching M_{octra}–O appears as peak positioned at 498 cm^{-1}. HR-SEM images confirms spherical nanoparticles with agglomerated nature for strontium doped zinc aluminate nanoparticles. The presence of oxygen, aluminium, zinc and magnesium elements were confirmed from EDX spectra. The band gap of $ZnAl_2O_4$ was found to be 5.16 eV and the bandgap increases gradually with the increase in Sr^{2+} doping concentration. The magnetization plots were determined the super paramagnetic behaviour at room temperature.

(Received November 15, 2021; Accepted March 15, 2022)

Keywords: Spinel nanoparticles, FT-IR analysis, UV-visible analysis, Paramagnetism.

1. Introduction

The spinel system has chemical formula AB_2O_4, where A denotes the divalent (A^{2+}) metal ion and B denotes the trivalent (B^{3+}) metal ion. Because of their exceptional mechanical resilience, excellent quantum yields, hydrophobic characteristics, vast surface area, low surface acidity, and thermal stability, they are used in a variety of applications such as sensors, electrodes, pigments, magnetic, optical, photocatalysts, refractories, and lubricant additives have all been widely used [1-6]. $ZnAl_2O_4$ also known as Gahnite, has three crystal structures: cubic, octahedral, and dodecahedral. Because of its spinal nature, it has increased chemical stability, thermal, mechanical and significantly. Zinc aluminate (spinel structure) has recently become popular in a variety of applications.

Rahman et al and Li et al. reported the photo catalytic and translucent aluminates synthesized by solid state and precipitation method. Esposito and Wang et al reported the thermodynamics and fluorescence application [7-10], which provides numerous benefits such as:

* Corresponding author: jrajabathar@ksu.edu.sa
https://doi.org/10.15251/JOR.2022.182.167

good mechanical and wide energy band gap, as well as at elevated temperature, resistant to the attack of chemicals, good thermal shock resistance. Zinc aluminates ($ZnAl_2O_4$) is found to be suitable for industrial applications viz. transparent armors, refractories, windows, IR domes and phosphor [11]. Chemical solution procedures have been widely used to create spinel nanoparticles in powder form. Various physical and chemical processes, including hydrothermal, co-precipitation, sol-gel, polymeric precursor and solid state reaction and so on can be used to make $ZnAl_2O_4$ spinel nanoparticles [12-14, 1].

The combustion approach, for example, has a number of benefits, including a shorter synthesis time, lower costs, and a larger yield of strontium doped zinc aluminate. In propellant chemistry, the fuel/oxidizers principle is used, using nitrates as precursors and l arginine as a fuel. Urea, L-alanine, citric acid, hydrazine and glycine, are some of the metal nitrates and fuels used in this process [15-17]. In the present study, Sr^{2+} doped $ZnAl_2O_4$ nanoparticles were produced by combustion method. XRD, FT-IR, UV-DRS, VSM, HR-SEM with EDX were used to investigate effects of divalent and trivalent metal ions and calcination temperatures on the structure, optical, magnetic vibrational properties and morphology of MAl_2O_4 (M = Zn), spinel nanoparticles.

2. Experimental procedure

2.1. Materials

Zinc nitrate hexahydrate ($Zn(NO_3)_2.6H_2O$, ≥ 98%), strontium nitrate hexahydrate ($Sr(NO_3)_2.6H_2O$ ≥ 98%), aluminum nitrate nonahydrate ($Al(NO_3)_3.9H_2O$, ≥ 99%) and L-arginine ($C_6H_{14}N_4O_2$, ≥ 98%) were used to synthesize $Zn_{1-x}Sr_xAl_2O_4$, (where x = 0, 0.1, 0.3 and 0.5) nanoparticles. All the chemicals purchased from Merck were of analytical grade and it was utilized as purchased. The samples were prepared with double distilled water.

2.2. Synthesis of $Zn_{1-x}Sr_xAl_2O_4$ Spinel Nanoparticles

To synthesize pure and strontium doped zinc aluminate nanoparticles, metal nitrates such as strontium nitrate, zinc nitrate, aluminum nitrate were taken as precursor materials and L-arginine was used as a fuel. To obtain a homogeneous solution, elements in desirable quantity was dissolved completely in de-ionized water followed by stirring for 30 minutes at room temperature. Based on propellant chemistry concept, the fuel-to-oxidizer ratio (F/O) was equal to one [20, 21]. The stirred consistent solution was discharged into silica crucible and kept at 550 °C for 2 h in a temperature-controlled muffle furnace. Final product slurry was cleaned repeatedly with ethanol and distilled water and dried at 100 °C for 2 h in an electric oven. The final obtained products were $ZnAl_2O_4$, $Sr_{0.1}Zn_{0.9}Al_2O_4$, $Sr_{0.3}Zn_{0.7}Al_2O_4$ and $Sr_{0.5}Zn_{0.5}Al_2O_4$ and the samples are labeled ZA, ZSA1, ZSA2, and ZSA3, respectively. Reaction mechanism during the process are as follows:

$$17Zn(NO_3)_2\,6H_2O_{(s)} + 34Al(NO_3)_3\,9H_2O_{(s)} + 20C_6H_{14}N_4O_{2(s)} \rightarrow 17\,ZnAl_2O_{4(s)} + 548H_2O_{(g)} + 12\,CO_{2(g)} + 108N_{2(g)} \quad (1)$$

2.3. Techniques

A Philips Expert X-ray diffractometer (XRD) were utilized to characterize the structural properties of pure and Sr doped $ZnAl_2O_4$. FTIR Spectrum spectrophotometer in the region of 400-4000 cm^{-1}, using KBr elements and the functional group present in pure and Sr doped $ZnAl_2O_4$ determine by FTIR. Morphological studies of pure and Sr doped $ZnAl_2O_4$ were carried out using a Jeol JSM6360 HR-SEM furnished with an energy dispersive X-ray analyzer (EDX) to identify the elemental composition. Energy band gap value of Sr doped $ZnAl_2O_4$ have been analyzed Agilent Cary 5000 UV-Vis spectrometer. The magnetic properties were measured at 300K using a Lakeshore VSM 7410 model outfitted with 3T magnets.

3. Result and Discussion

3.1. Powder XRD analysis

Fig.1 X-ray diffraction patterns of Sr^{2+} doped $ZnAl_2O_4$ spinel nanoparticles.

Fig. 1 displayed for the evolution of XRD patterns of Sr^{2+} doped $ZnAl_2O_4$ spinel nanoparticles. The structural phase formation of the synthesized spinel nanoparticles can be obtained from powder X-ray diffraction technique. Diffraction peaks of the synthesized $Zn_{1-x}Sr_xAl_2O_4$ ($0 \leq x \leq 0.5$) nanoparticles appear at 31.2°, 36.75°, 44.7°, 49.1°, 55.6°, 59.3°, 65.3°, 74.1°, and 77.3°. The corresponding peaks were matched with (220), (311), (400), (331), (422), (511), (440), (620), and (533) crystallographic planes of zinc aluminate spinels respectively. $ZnAl_2O_4$ crystal has spinel structure and belongs to the JCPDS card No: 05-0669, and $Fd\bar{3}m$ space group with a cubic symmetry. There were no added peaks noted, which confirms the implemented process is adequate to prepare ZnAl2O4 with single spinel phase structure.

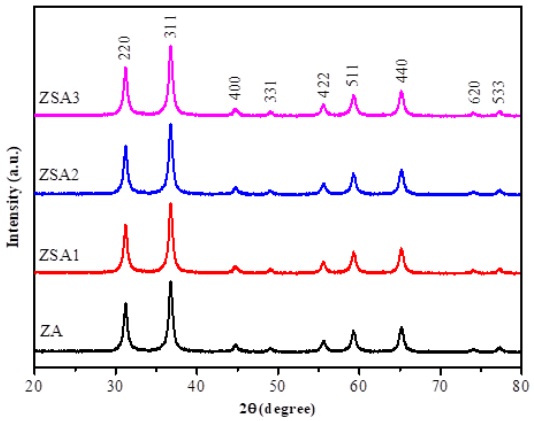

Fig. 1.Powder X-ray diffraction patterns of Sr^{2+} doped $ZnAl_2O_4$ spinel nanoparticles.

It is found that the diffraction peak (311) is shifted towards higher angle as Sr^{2+} doping concentration increases (Fig. 1). Combustion method well suitable for the synthesized samples as it produces the required phase of $ZnAl_2O_4$ and Sr^{2+} doped $ZnAl_2O_4$ spinel structure.

The Debye-Scherrer formula is used to calculate the average crystallite size (D) [18]:

$$D = \frac{0.89\lambda}{\beta \cos\theta} \tag{2}$$

where λ is the wavelength of the X-ray, θ is the Bragg diffraction angle and β is the full width at half maximum. The observed average crystallite size for cubic structure was found to be in the range 32 nm to 39 nm as shown in Table 1.

Table 1. Crystallite size, lattice parameter, cell volume and optical band gap of Sr^{2+} doped $ZnAl_2O_4$ spinel nanoparticles.

Sample Code	Crystallite size (nm)	Lattice parameter (Å)	Cell volume V ($Å^3$)	Band Gap (eV)	
ZA	32	8.0826	528.02	5.16	
ZSA1	35	8.0820	527.90	3.93	4.30
ZSA2	36	8.0815	527.80	3.95	4.34
ZSA3	39	8.0805	527.61	3.98	4.38

XRD data is used to calculate the lattice parameters of spinel phases in equ. (3) [1]:

$$\frac{1}{d^2} = \frac{h^2}{a^2} + \frac{k^2}{b^2} + \frac{l^2}{c^2} \tag{3}$$

where, d- inter-atomic spacing, *a*, *b* and *c* are the lattice constants, the results are noted (Table 1). It is noted that when Sr^{2+} concentration increases from x = 0 to 0.5, the lattice parameter values decreases and the equivalent cell volume (V) decreases. The radius of Sr^{2+} ion (r_{Sr}^{2+} = 1.44 Å) is found to be larger than Zn^{2+} ion (r_{Zn}^{2+} = 0.6 Å), whereas the lattice parameter and cell volume decreases. This corresponds to an increase in Al^{2+} ions average oxidation number which is due to the low valence Sr^{2+} ion [19, 20].

3.2. FT-IR analysis

In the synthesized samples, presence of functional groups with their characteristic peaks were obtained from FTIR spectra. Parameters such as unit cell, distances, oxygen bonding forces, cation distribution, and mass parameters etc., create an impact on the vibrational frequencies of aluminates. Fig. 2 depicts the vibrational spectrum containing $Zn_{1-x}Sr_xAl_2O_4$ spinel nanoparticles.

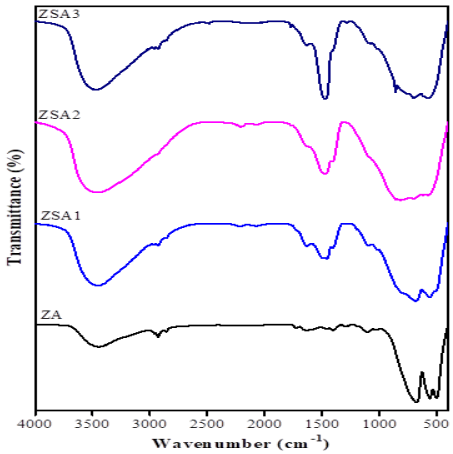

Fig. 2. FT-IR spectra of $Zn_{1-x}Sr_xAl_2O_4$ ($0 \leq x \leq 0.5$) samples.

The FTIR spectra was recorded between 400 and 4000 cm^{-1}. Stretching mode of hydroxyl molecule appear as a broad band at 3479 cm^{-1} and adsorption of hydroxyl molecule takes place at 1646 cm^{-1}. The band at 1477 cm^{-1} confirms the presence (H-O-H) bond vibration [1]. Three prominent peaks confirm the formation of spinel aluminate structure which are observed in the region 400-750 cm^{-1}. Pure zinc aluminates stretching frequencies of ν_1, ν_2, and ν_3 which appear around 710, 563 and 498 cm^{-1} respectively. The bands at 710 and 563 cm^{-1} indicates the intrinsic stretching vibrations of the M_{tetra}–O atom at the tetrahedral lattice sites and octahedral metal stretching M_{octra}–O appears as peak positioned at 498 cm^{-1} [21, 22]. It is clearly seen from the FTIR spectrum of $Zn_{1-x}Sr_xAl_2O_4$ ($0 \leq x \leq 0.5$) that as the concentration of Sr^{2+} ion in $ZnAl_2O_4$ increases, the frequencies ν_1, ν_2, and ν_3 seem to have shifted towards the higher wavenumber. This shift is due to lower molecular weight of the doped Sr^{2+} to that of Zn^{2+} ion.

3.3. UV-Vis analysis

The optical band gap of the synthesized pure $ZnAl_2O_4$ and Sr^{2+} doped $ZnAl_2O_4$ were obtained from UV-visible diffuse reflectance (UV-DRS) spectroscopy. Band gap of the synthesized materials are highly influenced by impurities, carrier concentration and lattice. Doping of a metal ion in the base matrix helps in tuning the band gap of the material thereby the synthesized material can be used for many applications. Linear extrapolation has been opted for n

= 2 indicate that $ZnAl_2O_4$ and Sr^{2+} doped $ZnAl_2O_4$ is a direct band gap semiconductor. The reflectance data of the synthesized samples were used in the Kubelka-Munk function to obtain the band gap of the synthesized materials. For that, the absorption coefficient was calculated from the reflectance data.

The absorption coefficient (α) is obtained from the equation,

$$\alpha = F(R) = \frac{(1-R)^2}{2R} \tag{4}$$

where, *F(R)* represents the Kubelka–Munk function and reflectance is denoted by R. Tau'c relation is used to compute the optical transition values by using the following equation:

$$\alpha h\nu = A\left(h\nu - E_g\right)^n \tag{5}$$

where, absorption coefficient is denoted by α, *A*- edge width parameter (Constant), E_g- energy band gap, n (n =1/2 for indirect and n = 2 direct optical band gap) is the constant dependent of degree of transition, where (*hν*)- energy of the photon. Using Tauc relation, by linear extrapolation, graph is plotted between the value of $(\alpha h\nu)^2$ on y-axis and (*hν*) on x-axis.

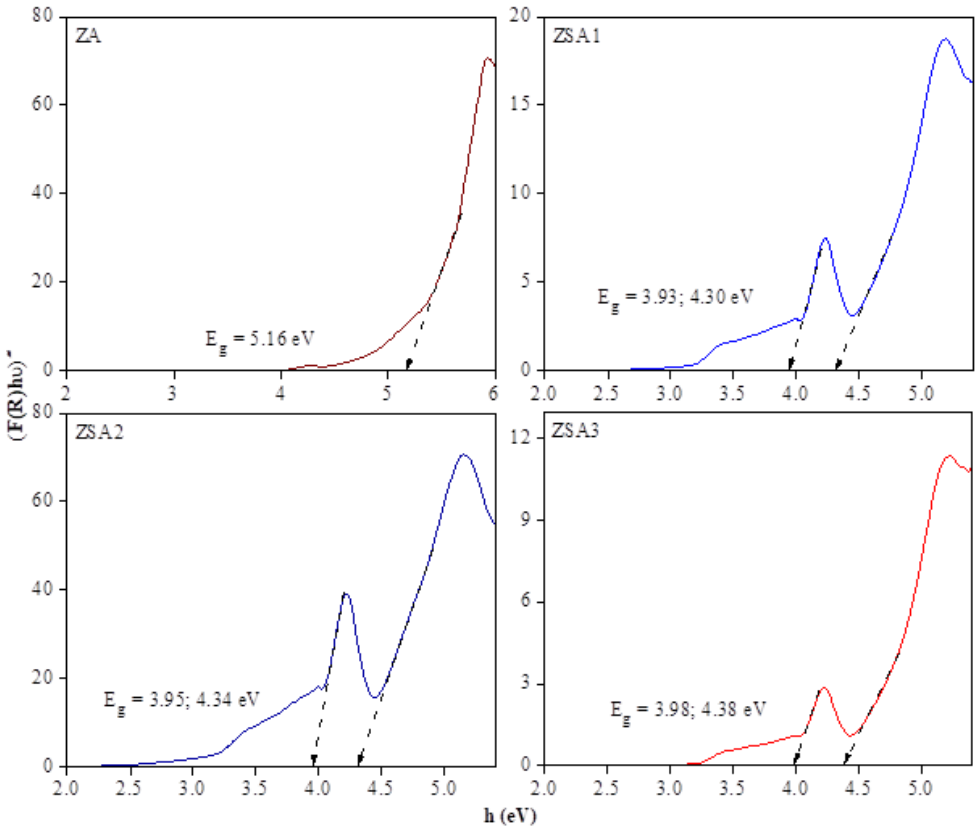

Fig. 3. Plot of $(F(R)h\nu)^2$ versus hν for Sr^{2+} doped $ZnAl_2O_4$ spinel nanoparticles.

Fig.3 depicts the plot of $(F(R)h\nu)^2$ versus *hν* of $Zn_{1-x}Sr_xAl_2O_4$ spinel nanoparticles. From the (Fig. 3) band gap of pure $ZnAl_2O_4$ was determined to be 5.16 eV is lower than the reported values of 5.50 eV which is due to the quantum confinement phenomena occurring at nano-regime. With increasing in alkaline Sr^{2+} ion doping with spinel materials, which was revealed two linear regions are observed. When Sr^{2+} content increases , it was found that band gap related to the first region was linearly increased such as 3.93 eV, 3.95 eV, and 3.98 eV, and the second region also increased 4.30 eV, 4.34 eV, and 4.38 eV, respectively [18, 19].

3.4. HR-SEM analysis

Fig. 4 illustrates the surface morphology and size of the grain can be obtained from HR-SE technique. In case of pure $ZnAl_2O_4$, particles were spherical in nature and seem to be agglomerated all over the surface.

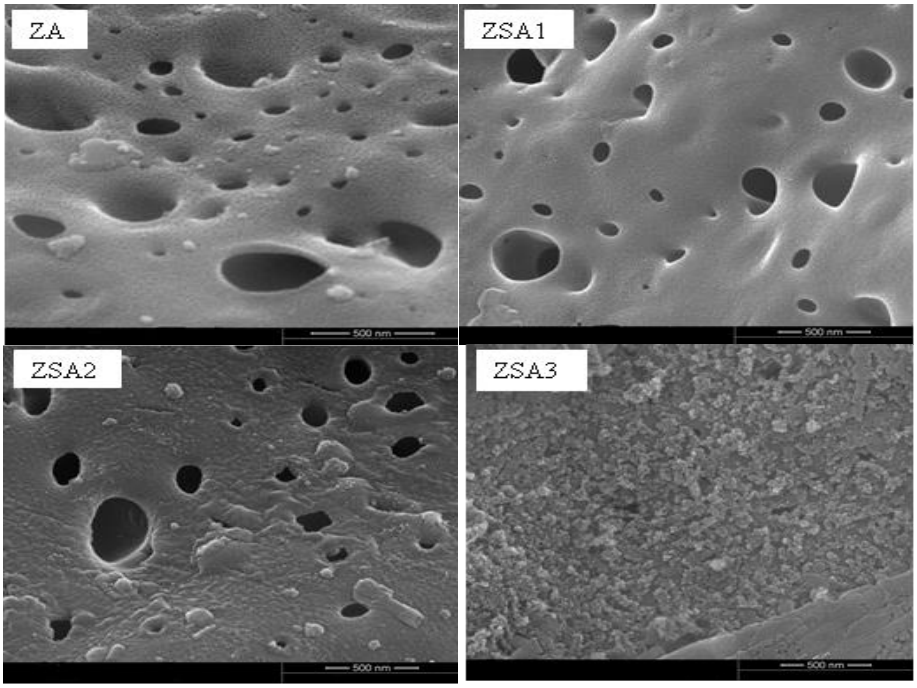

Fig. 4. HR-SEM images of $Zn_{1-x}Sr_xAl_2O_4$ ($0 \leq x \leq 0.5$) samples.

Further, the morphology is mainly affected by parameters like, synthesis method and presence of defects, which is due to increasing alkaline material of Sr^{2+} doping concentration. Pure $ZnAl_2O_4$ and $Zn_{0.9}Sr_{0.1}Al_2O_4$ exhibit similar morphology, whereas for $Zn_{0.7}Sr_{0.3}Al_2O_4$ agglomeration of the particles got reduced and finally $Zn_{0.5}Sr_{0.5}Al_2O_4$ nanoparticles exhibit uniform flake like structures.

3.5. EDX analysis

Elemental analysis technique is shown in Fig. 5 in order to check all of the unified elements are present in the synthesised nanoparticles. The quantitative spectra of a synthesised sample of $Zn_{1-x}Sr_xAl_2O_4$ ($0 \leq x \leq 0.5$) nanoparticles as well as atomic and weight percentages of all the elements, are given in the inset table.

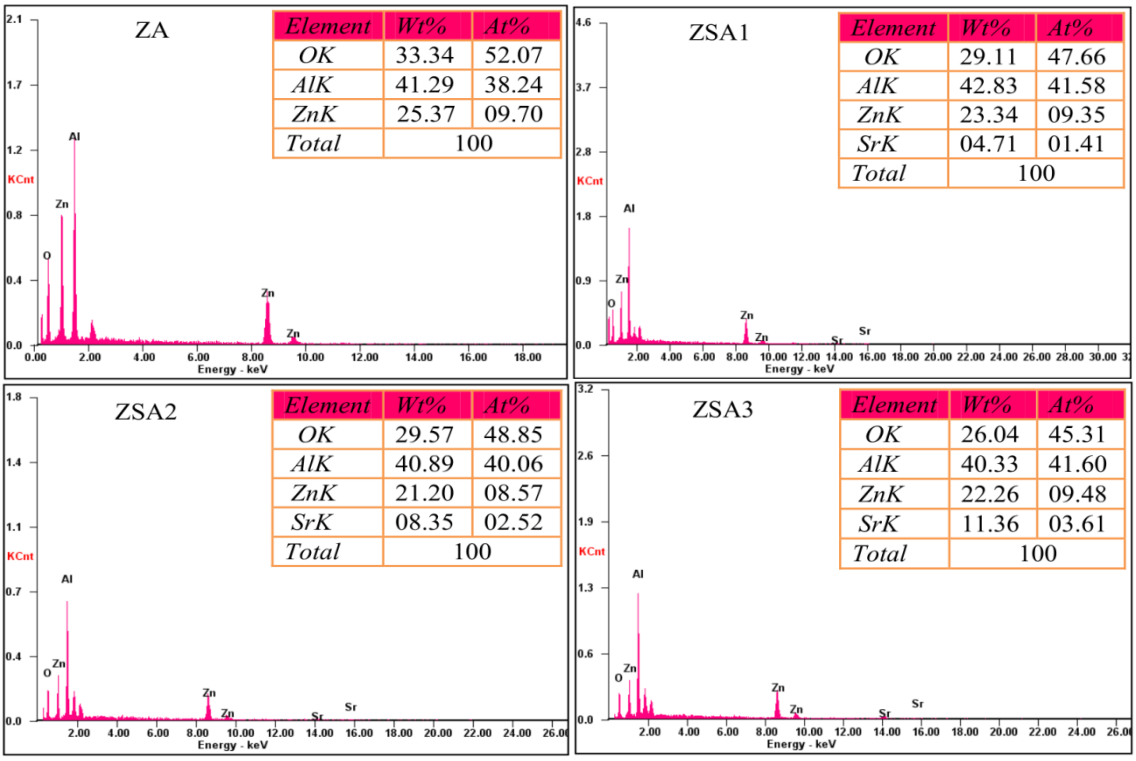

Fig. 5. EDX spectra of $Zn_{1-x}Sr_xAl_2O_4$ ($0 \leq x \leq 0.5$) samples.

Lack of impurities in EDX spectrum demonstrates high purity of the precursor. The presence of oxygen, aluminium, magnesium, and zinc is confirmed by EDX spectra. The observed Sr/Zn:Al molar ratios are all adjacent to 1:2, confirming the reagent ratios and M:Al stoichiometric ratios in $Zn_{1-x}Sr_xAl_2O_4$ samples.

3.6. VSM analysis

Vibrating sample magnetometer shows the magnetic properties of pure $ZnAl_2O_4$ and Sr^{2+} doped $ZnAl_2O_4$ spinel nanoparticles. The magnetization curves were measured from the field applied -15000 Oe to +15000 Oe and the graph is shown in Fig. 6, it determined the super paramagnetic behaviour. The plot depicted is a comparison of magnetization and magnetic field on y and x-axis respectively. From the graph, are determined coercivity, remanence and saturation values (Table 2).

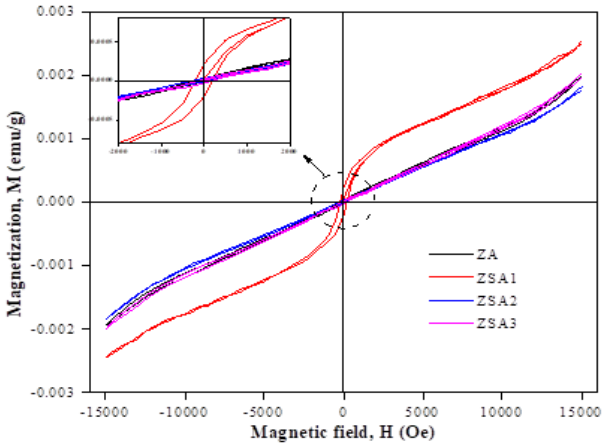

Fig. 6. Magnetic hysteresis curves of $Zn_{1-x}Sr_xAl_2O_4$ ($0 \leq x \leq 0.5$) samples.

The remanence values are initially increasing 20.70 to 201.47 emu/g, (x = 0 to 0.1) then decrease 20.87 emu/g (x = 0.3), finally increase 27.29 emu/g (x = 0.5). Further saturation values leads 1.96 emu/g, 2.49 emu/g for x = 0 to 0.1 then decrease 1.83 emu/g for x = 0.3 and leads 2.01 emu/g for x = 0.5.

Table 2. Magnetic parameters of Sr^{2+} doped $ZnAl_2O_4$ spinel nanoparticles.

Sample Code	Coercivity, Hc (Oe)	Remanence Mr, (μemu/g)	Saturation Magnetisation, Ms (memu/g)
ZA	139.11	20.703	1.9608
ZSA1	206.01	201.47	2.4961
ZSA2	170.94	20.874	1.8336
ZSA3	162.82	27.296	2.0115

Moreover, the variation is due to cationic distribution, particle size, and various compositions in strontium doped zinc aluminates [23]. The coercivity initially increase 139.11, 206.01 Oe for x = 0, 0.1 and decreases 170.94 Oe for x = 0.3 and 162.82 Oe for x = 0.5, its due to the behaviour is owing to the collaboration of metals with oxygen in sub-lattice and disruptions in the structure of the crystal lead to coercivity decreases [24].

4. Conclusion

Pure and Sr doped zinc aluminate nanoparticles were synthesized by combustion method. Structural confirmation was done from powder X-ray diffraction studies. Pure zinc aluminates have three main peaks close to stretching frequencies of ν_1, ν_2, and ν_3 which appear near 710, 563 and 498 cm^{-1} respectively. Spherical nanoparticles with agglomerated nature were seen from high resolution scanning electron microscopy. The EDX spectra checks the presence of oxygen, aluminium, zinc and magnesium elements. Band gap of pure $ZnAl_2O_4$ was found to be 5.16 eV is found to be lower than reported value of 5.50 eV. This is due to quantum confinement phenomena which occurs at nano-regime. The synthesized nanoparticles exhibit super paramagnetic behavior at room temperature is confirmed from Magnetization–Field (M−H) hysteresis curves.

Acknowledgments

The authors acknowledge the Researchers Supporting Project Number (RSP-2021/54) King Saud University, for financial supports, Riyadh, Saudi Arabia.

References

[1] J. Wrzyszcz, M. Zawadzki, J. Trawczyński, H. Grabowska, W. Miśta, Appl. Catal. A: Gen. 210, 263 (2001); https://doi.org/10.1016/S0926-860X(00)00821-8

[2] T. Maniecki, P. Mierczyński, W. Maniukiewicz, D. Gebauer, W. Jozwiak, Kinet. Catal. 50, 228 (2009); https://doi.org/10.1134/S0023158409020128

[3] K. M. de Souto Viana, B. B. Dantas, N. Nogueira, J. Sasaki, N. L. de Freitas, R. H. G. A. Kiminami, A. C. F. de Melo Costa, Mater. Sci. Forum 660-661, 52 (2010); https://doi.org/10.4028/www.scientific.net/MSF.660-661.52

[4] S. G. Menon, K. S. Choudhari, S. A. Shivashankar, S. Chidangil, S. D. Kulkarni, New J. Chem. 2017.

[5] T. Tangcharoen, J. T. Thienpraser, C. Kongmark, J. Adv. Ceram. 8(3), 352 (2019);

https://doi.org/10.1007/s40145-019-0317-5
[6] M. Agila, S. Krithiga, Int. j. eng. sci. manag. res. 2(2), 2581 (2019).
[7] A. Rahman, M. S Charoo, R. Jayaganthan, Adv. Perform. Mater. 30(3), 168 (2015); https://doi.org/10.1179/1753555714Y.0000000211
[8] J. G. Li, T. Ikegami, J. H. Lee, T. Mori, J. Am. Ceram. Soc. 83(11), 2866 (2010).
[9] L. Esposito, A. Piancastelli, P. Miceli, S. Martelli, J. Eur. Ceram. Soc. 35(2), 651 (2015); https://doi.org/10.1016/j.jeurceramsoc.2014.09.005
[10] S. F. Wang, G. Z. Sun, L. M. Fang, L. Lei, X. Xiang, X. T. Zu., Sci. Rep. 5(1), 1 (2015); https://doi.org/10.1038/srep12849
[11] A. E. Lavat, M. C. Grasselli, E. G. Lovecchio, Ceram. Int. 36(1), 15 (2010); https://doi.org/10.1016/j.ceramint.2009.06.015
[12] I. Miron, I. Grozescu, Optoelectron. Adv. Mat. 6, 673 (2012).
[13] C.-C. Yang, S.-Y. Chen, S.-Y. Cheng, Powder Technol. 148, 3 (2004); https://doi.org/10.1016/j.powtec.2004.09.011
[14] M. Valenzuela, P. Bosch, G. Aguilar-Rios, A. Montoya, I. Schifter, J. Sol-Gel Science and Tech. 8, 107 (1997); https://doi.org/10.1007/BF02436826
[15] Sofia N. Iyandurai, S. Yuvaraj, M. Sundararajan, Mater. Res. Express. 7, 046104 (2020); https://doi.org/10.1088/2053-1591/ab7a7a
[16] S. Baskar, S. Yuvaraj, M. Sundararajan, Chandra Sekhar Dash, Spinel. J. Supercond. Novel Mag., 1 (2020).
[17] A. T. Dhiwahar, M. Sundararajan, P. Sakthivel, C. S. Dash, S. Yuvaraj. J. Phy. Chem. Solids 138, 109257 (2020); https://doi.org/10.1016/j.jpcs.2019.109257
[18] M. Sukumar, L. J. Kennedy, J. J. Vijaya, B. Al-Najar, M. Bououdina, Mater. Sci. Semicond. Process 100, 225 (2019); https://doi.org/10.1016/j.mssp.2019.04.049
[19] G. T. Anand, L. J. Kennedy, J. J. Vijaya, K. Kaviyarasan, M. Sukumar, Ceram. Int. 41, 603 (2014); https://doi.org/10.1016/j.ceramint.2014.08.109
[20] M. Sukumar, L .J. Kennedy, J. J. Vijaya, B. Al-Najar, M. Bououdina, J. Magn. Magn. Mater. 465, 48 (2018); https://doi.org/10.1016/j.jmmm.2018.05.094
[21] T. Tangcharoen, I. T. Thienprasert, C. Kongmark, J. Adv. Ceram. 8(3), 352 (2019); https://doi.org/10.1007/s40145-019-0317-5
[22] M. Sukumar, L. J. Kennedy, J. J. Vijaya, B. Al-Najar, M. Bououdina, New J. Chem. 42, 18128 (2018); https://doi.org/10.1039/C8NJ04133D
[23] C. S. Dash, M. Kamalakannan, R. Jothi Ramalingam, H. Lohedan, S. Arokiyaraj, S. Yuvaraj, G. Anitha, A. Subramani, K. R. Sunaja Devi, M. Sundararajan, Digest J. Nanomaterials and Biostructures 16, 1287 (2021).
[24] M. Sundararajan, J. Vidhya, R. Revathi, M. Sukumar, V. Ravi, R. Rajkumar, M. Kamalakannan, C. S. Dash, H. Lohedani, R. Jothi Ramalingam, S. Arokiyaraj, J. Ovonic Research 17, 479 (2021).